Journal of Molecular Spectroscopy 319 (2016) 39–46

Contents lists available at ScienceDirect

Journal of Molecular Spectroscopy

journal homepage: www.elsevier.com/locate/jms

Rotational spectra of the Ne–N_2 complex based on a new three-dimensional potential energy surface using neural networks

Hong Fu [a,*], Rui Zheng [b,c], Limin Zheng [c]

[a] Department of Physical & Electrical Engineering, Ningde Normal University, Ningde 352100, People's Republic of China
[b] School of Mathematics & Information Science, North China University of Water Resources and Electric Power, Zhengzhou 450011, People's Republic of China
[c] Key Laboratory of Magnetic Resonance in Biological Systems, State Key Laboratory of Magnetic Resonance and Atomic and Molecular Physics, Wuhan Centre for Magnetic Resonance, Wuhan Institute of Physics and Mathematics, Chinese Academy of Sciences, Wuhan 430071, People's Republic of China

ARTICLE INFO

Article history:
Received 11 October 2015
In revised form 25 November 2015
Accepted 28 November 2015
Available online 18 December 2015

Keywords:
Ne–N_2
Potential energy surface
Neural networks
Bound state calculations
Spectroscopic parameters

ABSTRACT

A new three-dimensional potential energy surface (PES) of the Ne–N_2 van der Waals complex was constructed using the neural networks method based on *ab initio* data points at the CCSD(T) level. The aug-cc-pVQZ basis set was employed for all atoms, supplemented by midbond functions. The vibrationally averaged PES V_{00} is characterized by a global T-shaped minimum which occurs at $R = 3.385$ Å, $\theta = 90.0°$ with a well depth of -49.202 cm^{-1}. Based on our three-dimensional PES, bound state calculations were performed for four isotopologues, i.e. ^{20}Ne–$^{14}N_2$, ^{22}Ne–$^{14}N_2$, ^{20}Ne–$^{15}N_2$, ^{22}Ne–$^{15}N_2$, and several intermolecular vibrational states were assigned by analyzing the wavefunctions. Moreover, the averaged structural parameters were determined and the pure rotational transition frequencies with $J = 0$–5 are predicted. The spectroscopic constants were determined by fitting the rotational energy levels. The theoretical results are in good agreement with experimental data and this work gives more accurate results than those determined previously for the Ne–N_2 complex.

1. Introduction

The van der Waals complex is an ideal model in the research of intermolecular interactions, especially for the simple system consisting of a rare gas atom and a molecule. In the past decades, Ne–N_2 has been extensively investigated both experimentally [1] and theoretically [1–5].

For the Ne–N_2 complex, in experiment, in 1998, Jäger et al. [1] reported experimental high-resolution microwave spectra of the ground state ^{20}Ne–$^{14}N_2$, ^{20}Ne–$^{15}N_2$, ^{22}Ne–$^{14}N_2$, and ^{22}Ne–$^{15}N_2$ van der Waals complexes and the assignments of the observed transitions. In theory, in 1998, Jäger et al. [1] constructed a two-dimensional intermolecular PES at the CCSD(T) level of theory with basis sets aug-cc-pVTZ and aug-cc-pVQZ for ^{20}Ne–$^{14}N_2$ and ^{22}Ne–$^{14}N_2$. In 2001, an exchange-Coulomb (XC) potential energy model was developed for the Ne–N_2 interaction by Dham and Meath [2]. In 2003, Patel et al. [3] calculated intermolecular potentials for Rg–N_2 (Rg = He, Ne, and Ar) at the CCSD(T) level with basis sets aug-cc-pVTZ and aug-cc-pVDZ and obtained complete basis set limit surfaces using the Truhlar extrapolation formula. In 2004, Munteanu et al. [4] obtained a two-dimensional ground state PES with CCSD(T) and the aug-cc-pVXZ (X = 5, Q, T, D) basis sets augmented with two different sets of midbond functions. The aug-cc-pVQZ basis set results are close to the aug-cc-pV5Z results. In 2014, Baranowska-Łączkowska and Fernández [5] constructed two two-dimensional PESs at the CCSD(T) level with basis sets aug-pc-2-3321 and LPol-ds-33221.

For the Rg–N_2 (Rg = He, Ar, Kr, and Xe) complexes, several experimental [6–11] and theoretical studies [3,12–19] confirm that the stable structure of each complex is a T-shaped configuration.

In all the above PESs, the N_2 monomer was treated as a rigid rotor and the bound state calculated results are close to the experimental values. However, the three-dimensional PESs containing the intramolecular vibrations of the N_2 monomer are more accurate. For example, in 2011, Zhang et al. [20] developed a three-dimensional PES of the Kr–N_2 complex using the CCSD(T) method and mixed basis sets with midbond functions. They constructed five two-dimensional PESs at five values of N_2 bond length by fitting *ab initio* potential points to an analytic function, and then used the five two-dimensional PESs to construct the three-dimensional PES by interpolating. Compared to a two-dimensional PES of the Kr–N_2 complex [19], bound state calculations confirmed that a more accurate result could be obtained based on the three-dimensional PES. There is currently no report on the three-dimensional PES for the Ne–N_2 complex. Bechler [21] pointed out

* Corresponding author.
E-mail address: fuhongwipm@126.com (H. Fu).

http://dx.doi.org/10.1016/j.jms.2015.11.007
0022-2852/

that the PESs constructed using the neural networks (NN) methods are numerically very accurate and can be applied to different types of systems. In the present paper, we report a three-dimensional PES constructed using the neural networks method based on *ab initio* data points at the CCSD(T) level and bound state calculations. Also, this new three-dimensional PES containing the intramolecular vibrations of the N_2 monomer is very useful for the calculation of the infrared spectra of the Ne–N_2 complex.

2. Computational details

2.1. Ab initio calculations of intermolecular potential energy

The three-dimensional potential energy surface of the Ne–N_2 complex can be described by three Jacobi coordinates (R, θ, r), R is the distance between the rare gas atom and the center of mass of N_2, θ denotes the enclosed angle between the vector R and the molecular axis of N_2, and r is the N_2 bond length.

The *ab initio* potential energy grid for the Ne–N_2 complex was chosen as the following: the radial grid includes 18 points with the R coordinates {1.50, 2.00, 2.50, 2.75, 3.00, 3.10, 3.20, 3.30, 3.40, 3.50, 3.70, 4.00, 4.20, 4.50, 4.80, 5.00, 5.25, 6.00, 6.50, 7.00, 7.50, 8.00} Å, the N_2 bond length has five coordinates{0.80, 1.06, 1.0977, 1.12, 1.30} Å, and θ varies from 0° to 180° in steps of 15°.

The potential energy for each geometry was calculated using the supermolecular method at the level of single and double excitation coupled-cluster method with a noniterative perturbation treatment of triple excitations [CCSD(T)] [22]. The augmented correlation-consistent polarized valence quadruple-zeta (aug-cc-pVQZ) basis set of Dunning was employed for all atoms. The bond functions (3*s*3*p*2*d*2*f*1*g*) (for 3*s* and 3*p*, $\alpha = 0.94$, 0.34, 0.12; for 2*d* and 2*f*, $\alpha = 0.64$, 0.23; for 1*g*, $\alpha = 0.35$) [23] were also used at the middle point of the intermolecular distance R. The full counterpoise procedure of Boys and Bernardi [24] was employed to correct the basis set superposition error (BSSE). All the calculations were carried out using the Molpro 2010 software package [25].

2.2. Construction of the three-dimensional potential energy surface

Recently, a permutation invariant polynomial NN approach to fitting PES was proposed and successfully applied to the H + H_2, Cl + H_2, X + H_2O (X = H, O, and F) and OH + CO reaction systems by Jiang and Guo [26–28]. Chen and Zhang [29–32] constructed global PESs of chemical reaction systems such as H_2 + OH, OH + CO, H + CH_4, confirming that the NN fitting method is a powerful method to construct accurate PESs for polyatomic reactions. Here, we use the NN fitting method based on high level *ab initio* calculation to construct a three-dimensional PES of the Ne–N_2 van der Waals complex.

The architecture of feed-forward NN can be denoted *I*–*J*–*K*–1. Here, *I* is the number of nodes in the input layer, *J* and *K* are the number of neurons in the two hidden layers, and 1 is the number of neurons in the output layer. The value in the output layer, which is equal to potential energy of the input geometry can be calculated in the following way [29–31]:

The output of the *j*th neuron in the first hidden layer is

$$y_j^1 = f^1\left[b_j^1 + \sum_{i=1}^{I}\left(w_{j,i}^1 x_i\right)\right], \quad j = 1, 2, \ldots, J \tag{1}$$

The output of the *k*th neuron in the second hidden layer is

$$y_k^2 = f^2\left[b_k^2 + \sum_{j=1}^{J}\left(w_{k,j}^2 y_j^1\right)\right], \quad k = 1, 2, \ldots, K \tag{2}$$

The output in the output layer is

$$y = b_1^3 + \sum_{k=1}^{K}\left(w_{1,k}^2 y_k^2\right) \tag{3}$$

where $w_{j,i}^l$ denotes the weight connecting the *i*th neuron of $(l-1)$th layer and the *j*th neuron of *l*th layer, the b_j^l denotes the bias weight, where *l* indicates the layer of the target neuron and *j* its number, and the f^1 and f^2 are transfer functions taken as hyperbolic tangent functions. From Ref. [21], $x_i (i = 1, 2, 3)$ can be written as functions of Jacobi coordinates (R, θ, r) of Ne–N_2 van der Waals complex, the full symmetry is included in the NN,

$$x_1 = \left|\sqrt{R^2 + \left(\frac{m_1 r}{m_1 + m_2}\right)^2 - \frac{2m_1 R r\cos\theta}{m_1 + m_2}} + \sqrt{R^2 + \left(\frac{m_2 r}{m_1 + m_2}\right)^2 + \frac{2m_2 R r\cos\theta}{m_1 + m_2}}\right| \tag{4}$$

$$x_2 = \left|\sqrt{R^2 + \left(\frac{m_1 r}{m_1 + m_2}\right)^2 - \frac{2m_1 R r\cos\theta}{m_1 + m_2}} - \sqrt{R^2 + \left(\frac{m_2 r}{m_1 + m_2}\right)^2 + \frac{2m_2 R r\cos\theta}{m_1 + m_2}}\right| \tag{5}$$

$$x_3 = r \tag{6}$$

for Ne–$^{14}N_2$, m_1 and m_2 are the nuclear mass of ^{14}N. For Ne–$^{15}N_2$, m_1 and m_2 are the nuclear mass of ^{15}N.

The root mean squared error (RMSE) can be calculated to monitor the fitting accuracy,

$$\mathrm{RMSE} = \sqrt{\frac{1}{N_{data}}\sum_{i=1}^{N_{data}}\left(E_{fit} - E_{abinitio}\right)^2} \tag{7}$$

where N_{data} is the number of *ab initio* potential energy grids, which are divided into a training set (95%) and a validation set (5%), NN was trained using the Levenberg–Marquardt algorithm [33] to reduce the RMSE value and the "early-stopping" method [34] was used to stop over fitting. We achieve a PES $V(R, \theta, r)$ with RMSE of 0.0105 cm^{-1} using Chen's code [29–31] with the NN structure of 3–15–15–1.

2.3. Vibrationally averaged two-dimensional potential energy surface

From earlier reports [20,35–39], we know that the calculated results from a vibrationally adiabatic potential are in good agreement with the experimental results. The vibrationally averaged Ne–N_2 potential is expressed as follows [40],

$$V_{v'v}(R, \theta) = \left\langle \chi_{v'}(r) \middle| V(R, \theta, r) \middle| \chi_v(r) \right\rangle \tag{8}$$

$\chi_v(r)$ is the vibrational wavefunction of N_2, which satisfies the following equation,

$$\left[-\frac{1}{\mu_{N_2}}\frac{\partial^2}{\partial r^2} + V_{N_2}(r)\right]\chi_v(r) = E_{N_2}\chi_v(r) \tag{9}$$

where μ_{N_2} is the reduced mass of N_2, $V_{N_2}(r)$ is the potential-energy curve of N_2. This curve was constructed by executing a one-dimensional interpolation with the Lagrange polynomial formula which has been employed in the previous studies [41,42]. The potential energy for each *ab initio* point was calculated using the aug-cc-pVQZ basis set at the CCSD(T) level.

2.4. Bound state calculations

Within the vibrationally adiabatic approximation, the Hamiltonian of the Ne–N_2 complex in Jacobi coordinates can be written as:

$$\hat{H}_v = -\frac{1}{2\mu}\frac{\partial^2}{\partial R^2} + \frac{1}{2\mu R^2}(\hat{J}-\hat{j})^2 + B_v\hat{j}^2 + V_{vv}(R,\theta) \quad (10)$$

Table 1
Parameters for Ne–N_2 are used in the bound state calculations. The unit of R_{min} and R_{max} is bohr.

	J	j_{max}	$N_{Gauss-Legendre}$	N_{PODVR}	R_{min}	R_{max}
$^{20}Ne-^{14}N_2$	5	90	100	50	3.0	15.0
$^{22}Ne-^{14}N_2$	5	90	100	50	3.0	15.0
$^{20}Ne-^{15}N_2$	5	90	100	50	3.0	15.0
$^{22}Ne-^{15}N_2$	5	90	100	50	3.0	15.0

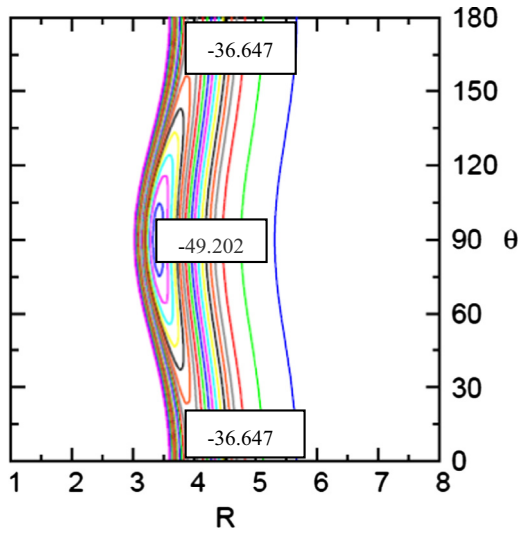

Fig. 1. Contour plots of the V_{00} PES for Ne–N_2; R is in angstrom, θ in degree and energy in cm^{-1}.

where μ is the reduced mass of the Ne–N_2 complex, $\hat{J}$ is total angular momentum and $\hat{j}$ is the angular momentum for N_2 monomer, and B_v is the rotational constant of N_2 with $B_0(^{14}N_2) = 1.989574$ cm^{-1}, and $B_0(^{15}N_2) = 1.857624$ cm^{-1} reported by Bendtsen [43].

The wave function of the system can be expanded as a linear combination of products of the radial and angular basis functions and written as:

$$\Psi(R,\theta) = \sum_i \sum_{j,K} c^i_{j,K}\varphi_i(R)Y^{JM\varepsilon}_{jK} \quad (11)$$

where $\varphi_i(R)$ is the radial basis function to describe the intermolecular stretch and obtained by solving a one-dimensional reference Hamiltonian defined as follows:

$$\hat{h} = -\frac{1}{2\mu}\frac{\partial^2}{\partial R^2} + V_{vv}(R,90^\circ) \quad (12)$$

ε is the index of the space-inverse parity of the system and $Y^{JM\varepsilon}_{jK}$ is the total symmetry-adapted angular basis function, which has the following explicit form,

$$Y^{JM\varepsilon}_{jK} = \frac{1}{\sqrt{2(1+\delta_{K0})}} \times \left[D^{*J}_{MK}(\alpha,\beta,\gamma)Y_{j,K}(\theta,0) + (-1)^{\varepsilon}D^{*J}_{M-K}(\alpha,\beta,\gamma)Y_{j,-K}(\theta,0)\right] \quad (13)$$

The total angular basis function is expressed in the body-fixed frame, where D^J_{MK} is a Wigner rotation matrix to describe the overall rotation of the complex. $Y_{j,K}(\theta,0)$ are the spherical harmonics, describing the rotation of N_2 monomer.

The bound state calculation program is OpenMP parallelized and the PARPACK software package [44] was applied to solve the eigenvalues and eigenfunctions of the bound states. The details of the bound state calculation method have been described previously [41,42]. Because of the symmetry of the N_2 molecule, the eigenfunctions of Ne–$^{14}N_2$ and Ne–$^{15}N_2$ can be labeled with indexes (ε, j) and are divided into 4 symmetry blocks: (+1, odd), (+1, even), (−1, odd), (−1, even). Each block can be solved separately. In the bound state calculations, two kinds of DVR grids were used for the corresponding basis functions [45] in Hamiltonian matrix integrals: (1) the potential-optimized discrete variable representation (PODVR) [46] for the intermolecular distance R and (2) the Gauss–Legendre quadrature were used for the angular. The parameters used in the bound state calculations for Ne–N_2 are listed in Table 1.

Table 2
Important geometries and their corresponding energies on different PESs for Ne–N_2 (R in angstrom and energy in cm^{-1}).

PES		Jäger[a]	XC-1[b]	MTE[c]	2d-aV5Z[d]
T-shaped global minimum	R	3.40	3.36	3.37	3.38
	Energy	−46.5	−50.0	−53.3	−49.51
Linear saddle point	R	3.97	3.95	3.93	3.95
	Energy	−33.4	−35.8	−39.3	−36.59
PES		2d-aVQZ[e]	aug-pc-2-3321[f]	LPol-ds-33221[g]	V_{00}
T-shaped global minimum	R	3.38	3.39	3.39	3.385
	Energy	−49.24	−49.36	−50.28	−49.202
Linear saddle point	R	3.95	3.96	3.96	3.945
	Energy	−36.77	−37.71	−37.29	−36.647

[a] Given from Ref. [1].
[b] Given from Ref. [2].
[c] Given from Ref. [3].
[d] PES constructed using aug-cc-pV5Z-33211 basis set given from Ref. [4].
[e] PES constructed using aug-cc-pVQZ-33221 basis set given from Ref. [4].
[f] PES constructed using aug-pc-2-3321 basis set given from Ref. [5].
[g] PES constructed using LPol-ds-33221 basis set given from Ref. [5].

Table 3
Intermolecular vibrational energy levels and frequencies (in cm^{-1}) for the $^{20}Ne–^{14}N_2$ complex supported by the V_{00} PES.

J	Energy	Freq.	(ε, j)	No. in block
$J = 0$	−30.93191	0.00000	(1, even)	1
	−23.25866	7.67325	(1, odd)	1
	−18.31034	12.62157	(1, even)	2
	−9.07847	21.85344	(1, odd)	2

Table 4
Average structural parameters for both $\sum^e(0)$ levels and $\Pi^e(1)$ levels of the Ne–N_2 complex (R in angstrom and angles in degree).

System	$\sum^e(0)$ levels		$\Pi^e(1)$ levels	
	$\langle R\rangle$	$\langle\theta\rangle$	$\langle R\rangle$	$\langle\theta\rangle$
$^{20}Ne–^{14}N_2$	3.649	63.682	3.620	67.304
$^{22}Ne–^{14}N_2$	3.644	63.767	3.616	67.357
$^{20}Ne–^{15}N_2$	3.642	64.116	3.616	67.513
$^{22}Ne–^{15}N_2$	3.638	64.204	3.611	67.568

3. Results and discussion

3.1. Ab initio PES

Fig. 1 displays the contour plots of intermolecular potential energy surface V_{00} for the Ne–N_2 complex. From Fig. 1, one can see that there are a global minimum and two equivalent linear saddle points. The global minimum is T-shaped and has a well depth of $-49.202\ cm^{-1}$ located at $R = 3.385$ Å and $\theta = 90.0°$. The two equivalent linear saddle points are located at $R = 3.945$ Å and $\theta = 0.0°$ or $\theta = 180.0°$ and are $12.555\ cm^{-1}$ above the global minimum. The geometries and energies of these special points for the Ne–N_2 complex are given in Table 2, including the previous results for comparison. As seen in Table 2, the global minimum on each PES corresponds to be a T-shaped structure, in agreement with the experimental result [1].

Compared with previously reported PESs, the potential energy of global T-shaped minimum of the V_{00} PES recovers the depth of about (105.8% for the PES constructed by Jäger [1], 98.4% for the XC-1 PES [2], 92.3% for the MTE PES [3], 99.4% for the 2d-aV5Z PES [4], 99.9% for the 2d-aVQZ PES [4], 99.7% for the aug-pc-2-3321 PES [5], 97.9% for the LPol-ds-33221 PES [5]). The difference in the R coordinate is 0.015 Å between the PES constructed by Jäger and the V_{00} PES, −0.025 Å between the XC-1PES and the V_{00} PES, −0.015 Å between the MTE PES and the V_{00} PES, −0.005 Å between the 2d-aV5Z PES and the V_{00} PES, −0.005 Å between the 2d-aVQZ PES and the V_{00} PES, 0.005 Å between the aug-pc-2-3321 PES and the V_{00} PES, and 0.005 Å between the LPol-ds-33221 PES and the V_{00} PES. We can see that the well depth and distance at the minimum energy configuration of the V_{00} PES is very close to that of the other PESs. The main features of the V_{00} PES containing the global minimum and linear saddle points are in good agreement with other existing PESs for Ne–N_2.

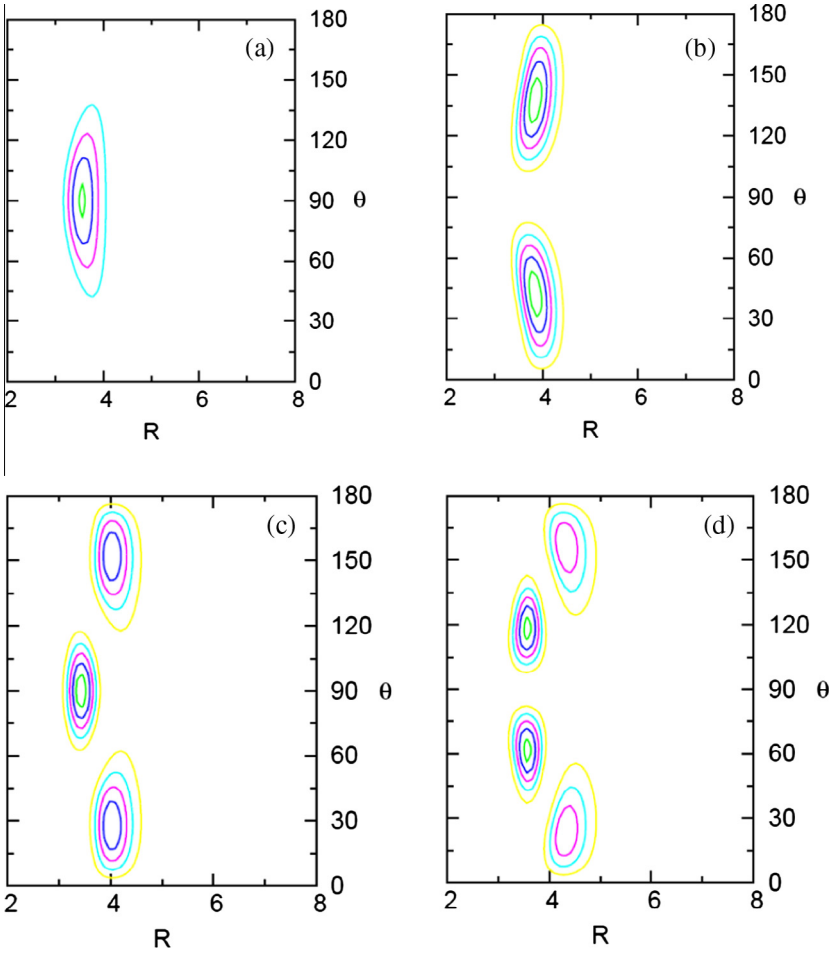

Fig. 2. Contour plots of the wavefunctions for the first four vibrational levels ($J = 0$) of $^{20}Ne–^{14}N_2$ supported by the V_{00} PES. The quantum number n denotes the intermolecular vibrational state. R is in angstrom and θ in degree. (a) $n = 0$; (b) $n = 1$; (c) $n = 2$; (d) $n = 3$.

3.2. Intermolecular vibrational states

The rovibrational energy levels and their corresponding wavefunctions for Ne–N_2 complex were obtained by performing bound state calculations. The energy levels, vibrational frequencies, their corresponding indices (ε, j), and the number of roots in block are summarized in Table 3 for the first four vibrational levels ($J = 0$) of ^{20}Ne–$^{14}N_2$ with V_{00} PES. The contour plots of the corresponding wavefunctions are shown in Fig. 2. From Fig. 2, we can see that intermolecular vibrational states (n) can, in general, not be assigned as the stretching mode and bending modes (n_s, n_b), because the wavefunctions are delocalized and vibrational modes are heavily mixed.

The ground state ($n = 0$) which is the 1st root in the (1, even) block is bound by energy $-30.931\ cm^{-1}$, indicating that the corresponding zero point energy is $18.271\ cm^{-1}$. Because the zero point energy is $5.716\ cm^{-1}$ higher than the barrier, the wavefunctions are delocalized and quantum tunneling occurs. The first excited vibrational state ($n = 1$) which has bound energy of $-23.259\ cm^{-1}$ is the 1st root in the (1, odd) block and corresponds to a bending excitation by analyzing the wavefunction. The bend vibrational frequency is $7.673\ cm^{-1}$. The second ($n = 2$) and third ($n = 3$) excited vibrational states are combination of stretching and bending modes.

3.3. Averaged structural parameters

The average structural parameters $\langle R\rangle$ and $\langle\theta\rangle$ for a vibrational state can be determined from the related wave functions using the following formulas [47]:

$$\left\langle \frac{1}{R^2} \right\rangle \approx \frac{1}{\langle R^2\rangle} \quad \text{and} \quad P_2(\cos\langle\theta\rangle) = \langle P_2(\cos\theta)\rangle \tag{14}$$

P_2 is the second order Legendre polynomial and $\langle P_2(\cos\theta)\rangle$ is the averaged value of the Legendre polynomial for the state of interest. The calculated structural parameters of the Ne–N_2 complex for both $\sum^e(0)$ levels and $\Pi^e(1)$ levels are listed in Table 4.

It is very interesting to compare the structural parameters for the minimum on the PES and the vibrational averaged values of ground state. For $\sum^e(0)$ levels, the intermolecular distances deviate slightly from the minimum on the PES, 0.264 Å for ^{20}Ne–$^{14}N_2$, 0.259 Å for ^{22}Ne–$^{14}N_2$, 0.257 Å for ^{20}Ne–$^{15}N_2$, and 0.253 Å for ^{22}Ne–$^{15}N_2$, respectively, reflecting the effects of zero-point motion.

Table 5
Calculated energies of pure rotational levels (in cm^{-1}) of the ^{20}Ne–$^{14}N_2$.

$J_{tot} = 0$		$J_{tot} = 1$		$J_{tot} = 2$		$J_{tot} = 3$		$J_{tot} = 4$		$J_{tot} = 5$	
0_{00}	−30.93191	1_{01}	−30.71657	2_{02}	−30.28623	3_{03}	−29.64150	4_{04}	−28.78335	5_{05}	−27.71309
		1_{11}	−27.92508	2_{12}	−27.51956	3_{13}	−26.91216	4_{14}	−26.10396	5_{15}	−25.09638
		1_{10}	−27.90765	2_{11}	−27.46721	3_{12}	−26.80731	4_{13}	−25.92883	5_{14}	−24.83300
				2_{21}	−22.63420	3_{22}	−22.01038	4_{23}	−21.17965	5_{24}	−20.14291
				2_{20}	−20.45168	3_{21}	−19.84853	4_{22}	−19.05298	5_{23}	−18.07356
						3_{31}	−19.84117	4_{32}	−19.03004	5_{33}	−18.01772
						3_{30}	−17.50041	4_{31}	−16.88252	5_{32}	−16.05893
								4_{41}	−14.48838	5_{42}	−13.39171
								4_{40}	−14.10153	5_{41}	−12.90820
										5_{51}	−9.12305
										5_{50}	−8.49554

Table 6
Calculated energies of pure rotational levels (in cm^{-1}) of the ^{22}Ne–$^{14}N_2$.

$J_{tot} = 0$		$J_{tot} = 1$		$J_{tot} = 2$		$J_{tot} = 3$		$J_{tot} = 4$		$J_{tot} = 5$	
0_{00}	−31.24708	1_{01}	−31.04259	2_{02}	−30.63389	3_{03}	−30.02156	4_{04}	−29.20644	5_{05}	−28.18971
		1_{11}	−28.25552	2_{12}	−27.86871	3_{13}	−27.28931	4_{14}	−26.51832	5_{15}	−25.55706
		1_{10}	−28.23990	2_{11}	−27.82180	3_{12}	−27.19532	4_{13}	−26.36124	5_{14}	−25.32068
				2_{21}	−22.96907	3_{22}	−22.37952	4_{23}	−21.59431	5_{24}	−20.61419
				2_{20}	−20.79479	3_{21}	−20.21990	4_{22}	−19.45916	5_{23}	−18.52107
						3_{31}	−20.21383	4_{32}	−19.44019	5_{33}	−18.47473
						3_{30}	−17.93959	4_{31}	−17.34534	5_{32}	−16.56022
								4_{41}	−14.92816	5_{42}	−13.89108
								4_{40}	−14.60194	5_{41}	−13.47832
										5_{51}	−9.72478
										5_{50}	−9.16511

Table 7
Calculated energies of pure rotational levels (in cm^{-1}) of the ^{20}Ne–$^{15}N_2$.

$J_{tot} = 0$		$J_{tot} = 1$		$J_{tot} = 2$		$J_{tot} = 3$		$J_{tot} = 4$		$J_{tot} = 5$	
0_{00}	−31.18394	1_{01}	−30.97400	2_{02}	−30.55441	3_{03}	−29.92577	4_{04}	−29.08899	5_{05}	−28.04527
		1_{11}	−28.40955	2_{12}	−28.01392	3_{13}	−27.42131	4_{14}	−26.63269	5_{15}	−25.64940
		1_{10}	−28.39279	2_{11}	−27.96359	3_{12}	−27.32050	4_{13}	−26.46436	5_{14}	−25.39633
				2_{21}	−23.12304	3_{22}	−22.51542	4_{23}	−21.70628	5_{24}	−20.69649
				2_{20}	−21.45280	3_{21}	−20.86344	4_{22}	−20.08486	5_{23}	−19.12411
						3_{31}	−20.85733	4_{32}	−20.06588	5_{33}	−19.07809
						3_{30}	−18.23139	4_{31}	−17.64884	5_{32}	−16.86473
								4_{41}	−15.54926	5_{42}	−14.48176
								4_{40}	−15.07255	5_{41}	−13.88762
										5_{51}	−10.10521
										5_{50}	−9.44413

Table 8
Calculated energies of pure rotational levels (in cm^{-1}) of the $^{22}Ne–^{15}N_2$.

$J_{tot}=0$		$J_{tot}=1$		$J_{tot}=2$		$J_{tot}=3$		$J_{tot}=4$		$J_{tot}=5$	
0_{00}	−31.50595	1_{01}	−31.30687	2_{02}	−30.90900	3_{03}	−30.313	4_{04}	−29.519	5_{05}	−28.529
		1_{11}	−28.74632	2_{12}	−28.36952	3_{13}	−27.805	4_{14}	−27.054	5_{15}	−26.117
		1_{10}	−28.73135	2_{11}	−28.32455	3_{12}	−27.715	4_{13}	−26.903	5_{14}	−25.891
				2_{21}	−23.46361	3_{22}	−22.890	4_{23}	−22.127	5_{24}	−21.174
				2_{20}	−21.80330	3_{21}	−21.241	4_{22}	−20.498	5_{23}	−19.580
						3_{31}	−21.236	4_{32}	−20.483	5_{33}	−19.542
						3_{30}	−18.661	4_{31}	−18.102	5_{32}	−17.357
								4_{41}	−15.995	5_{42}	−14.987
								4_{40}	−15.588	5_{41}	−10.694
										5_{51}	−10.090
										5_{50}	−9.306

The value of $\langle\theta\rangle$ reflects the amplitude of the bending vibration in the Ne–N_2 complex. The large deviations of $\langle\theta\rangle$ from their equilibrium values can be considered the effect of the hindered rotation of the N_2 monomer in the complex.

3.4. Rotational analysis

In this work, we use (v, n) to describe the vibrational state of the Ne–N_2 complex, v is the intramolecular vibrational state of the N_2 monomer and n is the intermolecular vibrational state of the Ne–N_2 complex. The energies of the rotational levels of the vibrational state $(v, n) = (0, 0)$ with $J = 0$–5 for $^{20}Ne–^{14}N_2$, $^{22}Ne–^{14}N_2$, $^{20}Ne–^{15}N_2$, and $^{22}Ne–^{15}N_2$ complexes were calculated and their assignments are listed in Tables 5–8. The theoretical transition frequencies of these complexes are listed in Tables 9 and 10. In Tables 9 and 10, the 2d-aVQZ represents a two-dimensional PES constructed using CCSD(T) and aug-cc-pVQZ basis set with a set of 3*s*3*p*2*d*2*f*1*g* midbond function, the 3d-aVQZ represents a three-dimensional PES using the same method and basis set as used in our work, Wang's two-dimensional PES [19] and Zhang's three-dimensional PES [20] of the $^{84}Kr–^{14}N_2$ complex were constructed using the CCSD(T) method; the basis sets were aug-cc-pVQZ-PP for the Kr atom and aug-cc-pVQZ for N atom. It can be seen that the *ab initio* calculated results of 2d-aVQZ and 3d-aVQZ are smaller than the experimental results and all the RMSEs

Table 9
Calculated microwave transition frequencies (in MHz) from 3d-aVQZ compared to experimental data and *ab initio* data from 2d-aVQZ for $^{20}Ne–^{14}N_2$ and $^{84}Kr–^{14}N_2$ complexes.

$J'_{K'_aK'_c}-J''_{K''_aK''_c}$	Expt.[a]	2d-aVQZ[b]	Calc.(2d)-expt.	3d-aVQZ[c]	Calc.(3d)-expt.
$^{20}Ne–^{14}N_2$					
$1_{01}–0_{00}$	6506.454	6451.3	−55.154	6455.721	−50.733
$2_{02}–1_{01}$	13003.574	12893.1	−110.475	12901.249	−102.325
$3_{03}–2_{02}$	19481.921	19316.0	−165.922	19328.490	−153.432
$4_{04}–3_{03}$	–	25710.1	–	25726.650	–
$2_{12}–1_{11}$	12274.323	12147.9	−126.423	12157.165	−117.158
$3_{13}–2_{12}$	18385.217	18195.3	−189.916	18209.366	−175.852
$4_{14}–3_{13}$	–	24210.6	–	24229.189	–
$2_{11}–1_{10}$	13303.809	13196.7	−107.108	13204.039	−99.770
$3_{12}–2_{11}$	19933.651	19772.8	−160.850	19783.274	−150.377
$4_{13}–3_{12}$	–	26322.0	–	26336.128	–
RMSE	–	137.411	–	127.505	–
$J'_{K'_aK'_c}-J''_{K''_aK''_c}$	Expt.[d]	2d-aVQZ[e]	Calc.(2d)-expt.	3d-aVQZ[f]	Calc.(3d)-expt.
$^{84}Kr–^{14}N_2$					
$2_{02}–1_{01}$	6035.269	5972.166	−63.103	5975.463	−59.806
$3_{03}–2_{02}$	9051.322	8956.599	−94.723	8961.696	−89.626
$4_{04}–3_{03}$	12065.473	11939.235	−126.238	11945.830	−119.643
$5_{05}–4_{04}$	15077.082	14917.973	−159.109	14927.566	−149.516
$2_{12}–1_{11}$	5951.889	5890.322	−61.567	5893.620	−58.269
$3_{13}–2_{12}$	8926.129	8833.984	−92.145	8838.781	−87.348
$4_{14}–3_{13}$	11898.319	11775.548	−122.771	11781.844	−116.475
$5_{15}–4_{14}$	14867.764	14712.914	−154.850	14722.508	−145.256
$2_{11}–1_{10}$	6091.215	6027.028	−64.187	6030.625	−60.590
$3_{12}–2_{11}$	9135.304	9039.342	−95.962	9044.439	−90.865
$4_{13}–3_{12}$	12177.568	12049.558	−128.010	12056.154	−121.414
$5_{14}–4_{13}$	15217.394	15056.177	−161.217	15065.770	−151.624
RMSE	–	115.918	–	109.403	–

[a] Given from Ref. [1].
[b] Given from Ref. [4].
[c] This work.
[d] Given from Ref. [10].
[e] Given from Ref. [19].
[f] Given from Ref. [20].

Table 10
Calculated microwave transition frequencies (in MHz) from 3d-aVQZ compared to experimental data and *ab initio* data from 2d-aVQZ for $^{22}Ne–^{14}N_2$ and $Ne–^{15}N_2$ complexes.

$J'_{K'_aK'_c}-J''_{K''_aK''_c}$	Expt.[a]	2d-aVQZ[b]	Calc.(2d)-expt.	3d-aVQZ[c]	Calc.(3d)-expt.
$^{22}Ne–^{14}N_2$					
$1_{01}–0_{00}$	6178.810	6126.5	−52.310	6130.447	−48.363
$2_{02}–1_{01}$	12349.261	12244.6	−104.661	12252.499	−96.762
$3_{03}–2_{02}$	18502.903	18345.7	−157.203	18357.164	−145.738
$4_{04}–3_{03}$	–	24421.0	–	24436.646	–
$2_{12}–1_{11}$	11706.171	11587.8	−118.371	11596.254	−109.917
$3_{13}–2_{12}$	17534.949	17357.1	−177.850	17369.948	−165.002
$4_{14}–3_{13}$	–	23096.5	–	23113.663	
$2_{11}–1_{10}$	12628.873	12527.6	−101.273	12534.304	−94.569
$3_{12}–2_{11}$	18923.640	18771.6	−152.041	18781.369	−142.271
$4_{13}–3_{12}$	–	24991.6	–	25005.051	–
RMSE	–	129.515	–	120.376	–
$^{20}Ne–^{15}N_2$					
$1_{01}–0_{00}$	6343.343	–	–	6293.833	−49.450
$2_{02}–1_{01}$	12677.932	–	–	12578.973	−99.021
$3_{03}–2_{02}$	18994.917	–	–	18846.124	−148.795
$4_{04}–3_{03}$	25285.249	–	–	25085.995	−199.254
$2_{12}–1_{11}$	11973.271	–	–	11860.671	−112.601
$3_{13}–2_{12}$	17935.576	–	–	17765.974	−169.602
$4_{14}–3_{13}$	23868.441	–	–	23642.196	−226.246
$2_{11}–1_{10}$	12964.231	–	–	12867.073	−97.158
$3_{12}–2_{11}$	19425.535	–	–	19279.324	−146.211
$4_{13}–3_{12}$	25861.611	–	–	25666.392	−195.219
RMSE	–	–	–	153.507	–
$^{22}Ne–^{15}N_2$					
$1_{01}–0_{00}$	6014.817	–	–	5968.259	−46.558
$2_{02}–1_{01}$	12021.828	–	–	11927.824	−94.004
$3_{03}–2_{02}$	18013.117	–	–	17872.400	−140.717
$4_{04}–3_{03}$	23980.632	–	–	23792.392	−188.240
$2_{12}–1_{11}$	11401.384	–	–	11296.163	−105.221
$3_{13}–2_{12}$	17080.371	–	–	16921.759	−158.611
$4_{14}–3_{13}$	22731.685	–	–	22519.775	−211.910
$2_{11}–1_{10}$	12287.430	–	–	12195.539	−91.891
$3_{12}–2_{11}$	18412.645	–	–	18274.721	−137.924
$4_{13}–3_{12}$	24515.455	–	–	24330.819	−184.637
RMSE	–	–	–	144.545	–

[a] Given from Ref. [1].
[b] Given from Ref. [4].
[c] This work.

Table 11
Comparision of spectroscopic parameters (in MHz) for Ne–$^{14}N_2$.

Parameter	^{20}Ne–$^{14}N_2$		^{22}Ne–$^{14}N_2$	
	Expt.[a]	This work	Expt.[a]	This work
A	69,778	69,778	69,676	69,676
B	3510.5628(31)	3489.3647	3319.9564(6)	3299.5608
C	2996.9450(31)	2967.1932	2859.8446(6)	2831.7668
Δ_J	0.26374(10)	0.26796	0.248006(19)	0.244841
Δ_{JK}	53.5173(20)	55.0931	45.29008(39)	46.59640
δ_J	0.035152(88)	0.035614	0.038720(17)	0.038719
H_J	–	–	–	–
H_{JK}	−0.10752(13)	−0.1120864	−0.093224(26)	−0.097670
Inertial defect (amu Å^2)	17.429	18.245	17.237	18.049

[a] Given from Ref. [1].

Table 12
Comparision of spectroscopic parameters (in MHz) for Ne–$^{15}N_2$.

Parameter	^{20}Ne–$^{15}N_2$		^{22}Ne–$^{15}N_2$	
	Expt.[a]	This work	Expt.[a]	This work
A	65,212	65,212	65,112	65,112
B	3419.406(16)	3398.578	3228.705(12)	3208.667
C	2924.871(16)	2896.240	2786.996(12)	2760.174
Δ_J	0.2389(11)	0.24092	0.22521(86)	0.22418
Δ_{JK}	52.1846(93)	53.6391	44.1514(74)	45.3857
δ_J	0.02949(22)	0.02904	0.03317(17)	0.03418
H_J	−0.000026(34)	0.000021	−0.000031(27)	−0.000068
H_{JK}	−0.10614(36)	−0.11017	0.09106(29)	−0.0943355
Inertial defect (amu Å^2)	17.240	18.042	17.046	17.831

[a] Given from Ref. [1].

of the 3d-aVQZ PESs are smaller than those of the 2d-aVQZ PESs with a value of about 10 MHz for Ne–$^{14}N_2$ and a value of about 7 MHz for ^{84}Kr–$^{14}N_2$, reflecting that the vibrationally averaged PESs of Ne–N_2 and ^{84}Kr–$^{14}N_2$ give more accurate results.

In order to compare the spectroscopic parameters with experimental values directly, the theoretical transition frequencies were fitted with the same Hamiltonian used in the experiment, namely a Watson asymmetric rotor expression employing the S-type reduction in the *Ir* representation [48],

$$H = \frac{1}{2}(B+C)J^2 + \left[A - \frac{1}{2}(B+C)\right]J_a^2 + \frac{1}{2}(B-C)\left(J_b^2 - J_c^2\right) - \Delta_J J^4 - \Delta_{JK} J_a^2 J^2 - \Delta_K J_a^4 + \delta_J J^2\left(J_+^2 - J_-^2\right) + \delta_K\left(J_+^4 - J_-^4\right) + H_J J^6 + H_{JK} J^4 J_a^2 + H_{kJ} J^2 J_a^4 + H_K J_a^6 \quad (15)$$

The determined parameters for Ne–$^{14}N_2$ and Ne–$^{15}N_2$ are listed in Tables 11 and 12, and show a good agreement with the corresponding experimental values. In Tables 11 and 12, the inertial defects are also listed. We can see that the calculated values of the inertial defects are a little larger than the corresponding experimental values, with the discrepancies of 0.816 amu Å^2 for the ^{20}Ne–$^{14}N_2$ complex, 0.812 amu Å^2 for the ^{22}Ne–$^{14}N_2$ complex, 0.802 amu Å^2 for the ^{20}Ne–$^{15}N_2$ complex, and 0.785 amu Å^2 for the ^{22}Ne–$^{15}N_2$ complex.

4. Conclusions

Ab initio calculations for the Ne–N_2 complex were performed using CCSD(T) and aug-cc-pVQZ basis sets for all atoms, supplemented by midbond functions (3*s*3*p*2*d*2*f*1*g*). Compared with previous PESs [1–5], the N_2 bond length was varied over five values, and the first three-dimensional PES for the Ne–N_2 complex was constructed using NN fitting method. By performing a potential integral, a vibrationally averaged two-dimensional PES was obtained. The vibrationally averaged PES V_{00} is characterized by a global T-shaped minimum, and two equivalent local linear saddle points.

Bound state calculations were performed for the ^{20}Ne–$^{14}N_2$, ^{22}Ne–$^{14}N_2$, ^{20}Ne–$^{15}N_2$, and ^{22}Ne–$^{15}N_2$ van der Waals complexes. Intermolecular vibrational states for ^{20}Ne–$^{14}N_2$ were assigned from the analysis of their wavefunctions. The average structural parameters were calculated and the pure rotational energy levels up to $J = 5$ were obtained. The theoretical rotational transition frequencies are compared with experimental values and previous results of other groups. The RMSEs between calculated and experimental results confirms the higher accuracy of our *ab initio* three-dimensional PES.

Acknowledgments

This work was supported by the Science Foundation for Introducing Talent of Ningde Normal University (Grant No. 2013Y004), the Education and Research Foundation (Science and Technology) for Young Teachers of the Education Department of Fujian Province (Grant No. JA15557), the Scientific Innovation Team Foundation of Ningde Normal University (Grant No. 2013T03), the National Science Foundation of China (Grant No. 21303254), and the National Natural Science Foundation of China (Grant No. 11304095). The authors thank Prof. Minghui Yang for providing the computer used to perform the calculations in this study.

References

[1] W. Jäger, Y. Xu, G. Armstrong, M.C.L. Gerry, F.Y. Naumkin, F. Wang, F.R.W. McCourt, J. Chem. Phys. 109 (1998) 5420.
[2] A.K. Dham, W.J. Meath, Mol. Phys. 99 (2001) 991.
[3] K. Patel, P.R. Butler, A.M. Ellis, M.D. Wheeler, J. Chem. Phys. 119 (2003) 909.
[4] C.R. Munteanu, J.L. Cacheiro, B. Fernández, J. Chem. Phys. 120 (2004) 9104.
[5] A. Baranowska-Łączkowska, B. Fernández, J. Comput. Chem. 35 (2014) 199.
[6] G. Henderson, G.E. Ewing, Mol. Phys. 27 (1974) 903.
[7] A.R.W. McKellar, J. Chem. Phys. 88 (1988) 4190.
[8] W. Jäger, M.C.L. Gerry, Chem. Phys. Lett. 196 (1992) 274.

[9] W. Jäger, M.C.L. Gerry, C. Bissonnette, F.R.W. McCourt, Faraday Discuss. 97 (1994) 105.
[10] W. Jäger, Y. Xu, N. Heineking, M.C.L. Gerry, J. Chem. Phys. 99 (1993) 7510.
[11] Q. Wen, W. Jäger, J. Chem. Phys. 122 (2005) 214310.
[12] Z. Slanina, S.J. Kim, K. Fox, J. Mol. Struct.: Theochem. 288 (1993) 17.
[13] F.Y. Naumkin, Mol. Phys. 90 (1997) 875.
[14] B. Fernández, H. Koch, J. Makarewicz, J. Chem. Phys. 110 (1999) 8525.
[15] C.R. Munteanu, J.L. Cacheiro, B. Fernández, J. Chem. Phys. 121 (2004) 10419.
[16] J. Zhu, Y.-P. Lu, X.-R. Chen, Y. Cheng, Eur. Phys. J. D 33 (2005) 43.
[17] A.K. Dham, W.J. Meath, J.W. Jechow, F.R.W. McCourt, J. Chem. Phys. 124 (2006) 034308.
[18] A.K. Dham, W.J. Meath, Chem. Phys. 196 (1995) 125.
[19] Z. Wang, M. Niu, E. Feng, H. Yu, J. Du, J. Ma, Chem. Phys. Lett. 484 (2010) 124.
[20] C. Zhang, Z. Wang, E. Feng, Chem. Phys. Lett. 517 (2011) 16.
[21] J. Bechler, Phys. Chem. Chem. Phys. 13 (2011) 17930.
[22] C. Hampel, K. Peterson, H.J. Werner, Chem. Phys. Lett. 190 (1992) 1.
[23] R.R. Toczylowski, S.M. Cybulski, J. Chem. Phys. 112 (2000) 4604.
[24] S.F. Boys, F. Bernardi, Mol. Phys. 19 (1970) 553.
[25] H.-J. Werner, P.J. Knowles, G. Knizia, F.R. Manby, M. Schütz, P. Celani, T. Korona, R. Lindh, A. Mitrushenkov, G. Rauhut, K.R. Shamasundar, T.B. Adler, R.D. Amos, A. Bernhardsson, A. Berning, D.L. Cooper, M.J.O. Deegan, A.J. Dobbyn, F. Eckert, E. Goll, C. Hampel, A. Hesselmann, G. Hetzer, T. Hrenar, G. Jansen, C. Köppl, Y. Liu, A.W. Lloyd, R.A. Mata, A.J. May, S.J. McNicholas, W. Meyer, M.E. Mura, A. Nicklaß, D.P. O'Neill, P. Palmieri, D. Peng, K. Pflüger, R. Pitzer, M. Reiher, T. Shiozaki, H. Stoll, A.J. Stone, R. Tarroni, T. Thorsteinsson, M. Wang, MOLPRO, Version 2010.1, a Package of Ab Initio Programs, 2010. <http://www.molpro.net>.
[26] B. Jiang, H. Guo, J. Chem. Phys. 139 (2013) 054112.
[27] J. Li, B. Jiang, H. Guo, J. Chem. Phys. 139 (2013) 204103.
[28] J. Li, J. Chen, D.H. Zhang, H. Guo, J. Chem. Phys. 140 (2014) 044327.
[29] J. Chen, X. Xu, X. Xu, D.H. Zhang, J. Chem. Phys. 138 (2013) 154301.
[30] J. Chen, X. Xu, X. Xu, D.H. Zhang, J. Chem. Phys. 138 (2013) 221104.
[31] X. Xu, J. Chen, D.H. Zhang, Chin. J. Chem. Phys. 27 (2014) 373.
[32] W. Koch, D.H. Zhang, J. Chem. Phys. 141 (2014) 021101.
[33] M.T. Hagan, M.B. Menhaj, IEEE Trans. Neural New. 5 (1994) 989.
[34] W.S. Sarle, in: Proceedings of the 27th Symposium on the Interface of Computing Science and Statistics, Interface Foundation of North America, Pittsburgh, 2005, p. 352.
[35] T.B. Pedersen, J.L. Cacheiro, B. Fernández, H. Koch, J. Chem. Phys. 117 (2002) 6562.
[36] K.A. Peterson, G.C. McBane, J. Chem. Phys. 123 (2005) 084314.
[37] Z. Wang, M. Gong, Y. Zhang, E. Feng, Z. Cui, Chem. Phys. Lett. 454 (2008) 7.
[38] E. Feng, Y. Zhang, Z. Wang, M. Niu, Z. Cui, J. Chem. Phys. 13 (2009) 124311.
[39] Z. Wang, E. Feng, H. Yu, C. Zhang, J. Du, J. Chem. Phys. 134 (2011) 024320.
[40] B.K. Taylor, R.J. Hinde, J. Chem. Phys. 122 (2005) 074308.
[41] L.M. Zang, W. Dai, L.M. Zheng, C.X. Duan, Y.P. Lu, M.H. Yang, J. Chem. Phys. 140 (2014) 114310.
[42] H. Fu, J. Lv, L.M. Zheng, R. Zheng, J. Mol. Spectrosc. 311 (2015) 100.
[43] J. Bendtsen, J. Raman Spectrosc. 2 (1974) 133.
[44] R. Lehoucq, D.C. Sorensen, C. Yang, ARPACK User's Guide: Solution of Large-Scale Eigenvalue Problems with Implicitly Restarted Arnoldi Methods, SIAM, Philadelphia, PA, 1998. <http://www.caam.rice.edu/software/ARPACK>.
[45] R.B. Lehoucq, S.K. Gray, D.H. Zhang, J.C. Light, Comput. Phys. Commun. 109 (1998) 15.
[46] J. Echave, D.C. Clary, Chem. Phys. Lett. 190 (1992) 225.
[47] H. Ran, Y.Z. Zhou, D.Q. Xie, J. Chem. Phys. 126 (2007) 204304.
[48] M.J. Weida, J.M. Sperhac, D.J. Nesbitt, J.M. Hutson, J. Chem. Phys. 101 (1994) 8351.